ACCEPTED MANUSCRIPT • OPEN ACCESS

A portable triaxial cell for beamline imaging of rocks under triaxial state of stress

To cite this article before publication: Amer Syed *et al* 2021 *Meas. Sci. Technol.* in press https://doi.org/10.1088/1361-6501/abeb94

A portable triaxial cell for beamline imaging of rocks under triaxial state of stress

Amer Syed
School of Engineering, University of Aberdeen, AB24 3UE, UK.
E-mail: amer.syed07@alumni.imperial.ac.uk

Yukie Tanino
School of Engineering, University of Aberdeen, AB24 3UE, UK.

Jacob M. LaManna
Physical Measurement Laboratory, National Institute of Standards and Technology, Gaithersburg, MD, USA.

David L. Jacobson
Physical Measurement Laboratory, National Institute of Standards and Technology, Gaithersburg, MD, USA.

Daniel S. Hussey
Physical Measurement Laboratory, National Institute of Standards and Technology, Gaithersburg, MD, USA.

Eli Baltic
Physical Measurement Laboratory, National Institute of Standards and Technology, Gaithersburg, MD, USA.

Genoveva Burca
STFC, Rutherford Appleton Laboratory, ISIS Facility, Harwell OX11 0QX, UK.
Faculty of Science and Engineering, The University of Manchester, M13 9PL, UK

January 2020

Abstract. With recent developments in direct imaging techniques using x-ray and neutron imaging, there is an increasing need for an efficient design of a test setup to study mechanical and/or the transport behaviour of porous rocks. Bespoke design from commercial suppliers are expensive and often difficult to modify. This paper presents a novel design of a portable triaxial cell for imaging deformation (and suggestion for adaptation for introducing fluid transport) through rocks/sand/soil under triaxial state of stress representative of those encountered in case of ground water aquifers or subsurface hydrocarbon reservoirs. The design philosophy and the parameters are detailed so that interested researchers can use this experimental set up as a template to design and modify the triaxial cell to suit their own experimental requirements. The design has been used on two imaging beamlines- IMAT, ISIS facility, Harwell, Oxfordshire, UK and BT2 of National Institute of Standards and Technology (NIST) Center for Neutron Research, Gaithersburg, MD, USA. The mass attenuation coefficients extracted from the 2D radiograms of the triaxial cell were compared with those reported in the literature. Further suggestions for the adaptation of triaxial cell for studying mechanics of deformation and fracture in rocks are included.

Keywords: neutron imaging, x-ray imaging, rock mechanics, triaxial cell.

1. Introduction

Parallel and cone beam imaging techniques have been increasingly adapted from medical science into other disciplines to address a wide range of scientific problems [1] including those in metrology [2], complex fluids [3], specific engineering problems such as cavitation [4] and non-destructive testing of components such as O-rings [5]. One such field that has benefited from th computed tomography is geosciences and geo-engineering with notable application being the study of flow through porous rocks [6, 7, 8, 9, 10, 11]. 2D radiograms obtained from neutron imaging can be used to estimate the porosity (to some extent) and to identify permeable pathways [12, 13] which are often due to increase in the length of cracks [14, 15]. Prior to the application of parallel or cone beam imaging, observations were primarily derived from bulk measurements or 2D imaging techniques such as Scanning Electron Microscopy (SEM) or Transmission Electron Microscopy (TEM) of thin rock sections. Using these imaging techniques, one is able to resolve micron to submicron level details of the grain structure or mechanics but, it is not possible to infer any information of the 3D geometrical features, which are significant in defining the mechanical behaviour of geomaterials. Furthermore, preparation of specimen, for thin section, may introduce artifacts, that could potentially limit the interpretation of experimental observations. Another important aspect that is neglected in case of SEM/TEM, is the reference to *in-situ* stresses (as it is the natural state of rock in the subsurface). With the exception of a few hard rocks (e.g. granite), most of the sedimentary rocks such as sandstone are compressible and the granular assembly of the rocks undergoes deformation with the application/release of stress.

The rock mass in the subsurface environment will be subjected to triaxial state of stress, which are:

(a) vertical stress, σ_{v}, resulting from the overlying rock mass of density ρ, accumulated over a depth of h, often termed as the overburden, and with the acceleration due to gravity g, is theoretically defined as

$$\sigma_{\mathrm{v}} = -g \int \rho \mathrm{d}h + \sigma_{\mathrm{t}}, \tag{1}$$

where σ_{t} is the magnitude of tectonic stress, if any, in the region; and

(b) horizontal stresses.

For many subsurface reservoir conditions, the two horizontal stresses are equal for all practical purposes. Hence, the selected shape of the rock sample is cylindrical, wherein the horizontal stress is applied through oil/water or gas on the cylindrical surface and the vertical stress is applied on the flat ends and along the longitudinal axis of the sample. The conventional design of the cells such as one proposed by [16] is too large with relatively complex hydraulics that limits its use for beamline imaging. To address this limitation, the current work discusses the design and application of a novel triaxial cell which requires space smaller than the conventional cell, facilitates easy removal of sample and is based on simple design philosophy that establishes a framework for designs of such triaxial cells that can be easily adapted to suit various requirements in relation to beamline parameters and state of stress in the sample.

Typically, the standard triaxial test carried out on rocks (porous as well as non-porous), is aimed at obtaining three pieces of information (a) the variation of stress induced in the sample on application of known strain, which, for elastic rocks, provides the basis for the measurement of elastic modulus, (b) Poisson's ratio, to relate the longitudinal compression of the rock sample with radial expansion and (c) the ultimate compressive stress, which can then be used to obtain the failure envelope of the rock. While these macroscopic parameters are measured and have been used to characterise rock, the microscopic observations of grain-grain or grain-binding material interactions including relative deformation and damage were not directly observed, partly due to limitations of the technology till date. Figure 1 depicts a typical output from a triaxial test, normally carried out at a constant strain rate. σ_1 and ϵ_1 are longitudinal stress and strain, σ_2 is the confining stress representing the horizontal stresses. The application of load supplies the strain energy necessary for the initiation and propagation of microcracks which would then further develop resulting in the failure of the material. The current design of the proposed triaxial cell enables the direct observation of the deformation at granular level amongst other observations (i.e. shear bands) of interest.

2. Basis of the design and the key parameters

The subject of mechanical design is multifaceted and now increasingly multidisciplinary in nature [17]. The approach to the current design derives its principles from radiation physics, material science, mechanical engineering and geological sciences. Often such multidisciplinary project teams comprise of participants less familiar with the design philosophy wherein the identification of information sources and their appropriate use is critical to the success of the designed product [18]. An effective design should always be based on the *key parameters* that could clearly distinguish *good* design from a *bad* one [19]. There are three key design parameters for the triaxial cell for imaging:

(a) the flux of the particles and their energy,

(b) the maximum load intended to be applied on the rock and,

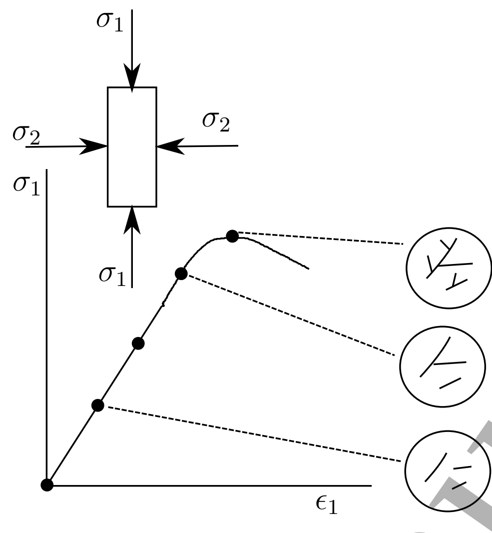

Figure 1. Schematic depicting the development of the crack network in a sample subjected to increasing stress under triaxial conditions. The insets show an idealised microscopic phenomena of initiation, development and coalescing of microcracks with increase in the applied strain.

(c) the design or safety factor.

For most beamlines, the flux is fixed and the attenuation of the particles is to be minimised. In some cases, the thickness of the material which the neutron beam/x-rays have to pass cannot be controlled, which warrants application of additional techniques such as combining stacks of multiple energies [20]. For the current design of the cell, the wall thickness of the cell and the diameter of the sample would dictate the attenuation of particles and the maximum stress that can be applied based on the design considerations. The trade off for item (b) above would be prescribed by the constraints imposed by items (a) and (c) above.

2.1. Constraints from the beamline facilities

X-ray and neutron imaging beamlines are widely used in the field of material characterisation, and more recently of geomaterials. X-ray and neutrons provide complementary information, thus informing the nature of the material investigated [21]. While x-rays, especially from a synchrotron source, enable images of higher resolution to be captured, neutrons on the other hand are suitable in probing lighter elements such as hydrogen and can be used to investigate thicker sample materials. This property of neutrons helps the imaging of geomaterials containing hydrogen rich fluids such as water and oil. Furthermore, x-ray imaging of rock-fluid interaction requires the fluid to be doped with potassium iodide- specially if multiple fluids are present in the pore spaces, which can be avoided if neutron imaging is used.
With minor variation, imaging experiments consists of acquisition of 2D radiograms of the sample placed on a rotating table in the the beamline. The attenuated radiation (I) can be computed using the sample of density, ρ and thickness, x, and mass-attenuation

coefficient μ/ρ (μ is the linear attenuation coefficient) and incident radiation (I_o) as [22]

$$I = I_o \exp\left[-(\mu/\rho)\rho x\right]. \tag{2}$$

In case the sample placed in the beamline is made of n different elements, Equation 2 can be modified as

$$\ln\left[\frac{I}{I_o}\right] = -\sum_i^n \left(\frac{\mu}{\rho}\right)_i \rho_i x_i. \tag{3}$$

The attenuation of four elements will be of interest in the current context of imaging rocks enclosed in a triaxial cell: Aluminium in the various components of the triaxial cell, Iron in the the fixtures (e.g. bolts), Silicon in the grains of rock and Carbon, if the pore space in rocks is saturated with organic materials such as hydrocarbons. For the purposes of comparison, the mass attenuation coefficient along with their specific densities are given in table 1 and will be used in the analysis of data later. It is to be noted that for the beamlines discussed the λ is centred around 1.8$\mathring{A}$ for BT2 and the maximum flux at IMAT is around 2.6$\mathring{A}$ and the coefficients reported in [22] corresponds to an approximate $\lambda = 1.08\mathring{A}$. For the design of x-ray and neutron transparent triaxial

Table 1. Selected properties of C, Al, Si and Fe for neutrons ($\lambda = 1.08\mathring{A}$) and x-ray (90 keV).

Element	μ/ρ neutron [cm^2 g^{-1}] [22]	μ/ρ x-ray [cm^2 g^{-1}] [23]‡	ρ [g cm^{-3}] [23]
Al	0.04	0.186	2.699
Fe	0.2	0.484	7.874
Si	0.045	0.203	2.33
C	0.3	0.156	1.7

cell, it is vital to assess the mass attenuation coefficient for the system. Commercially available triaxial cells are either made of carbon fibre composites [10] or Aluminium, with the later being the cheaper alternative. Commercially available core holders are used to study pore scale flow and not localised deformation. An important aspect is although carbon can be readily used as a sample holder for neutron imaging, carbon fibre composite are unsuitable due to high hydrogen content in the epoxy resin used in the manufacture. A simple design of x-ray transparent Aluminium cell was detailed by Fussels *et. al.* [24]. Aluminium has a few distinct advantages over carbon in addition to favourable mass attenuation coefficient for neutrons. Aluminium alloys are cheaper, easy to machine and readily recyclable after their use, thus making it a sustainable option.

2.2. Constraints imposed by the the rocks to be tested

Most rocks used in the construction industry as well as those investigated for oil and gas, such as sandstones, are consolidated and exhibit near perfect elastic behaviour with brittle mode of fracture. However, with the interest in non-conventional hydrocarbon recovery, rocks with complex mechanical behaviour, such as shales, are being studied with interest. Broadly, two types of minerals affect the degree of brittleness within the rocks: a) Quartz impart brittleness in the rocks resulting in small elastic strain when loaded in compression, prior to failure, and b) clay imparting ductility and resulting in larger strains. Therefore rocks containing these two minerals exhibit the behaviour of dominating mineral i.e sandstones are brittle as the dominating mineral is quartz whereas the mechanical behaviour of shale would depend on whether quartz or clay is the dominant mineral. Hence, the design of the cell needs to take into account the possible failure of the rocks that are intended to be tested.

2.3. Factor of safety

Factor of Safety (FoS) is included to ensure the equipment is safely operated. FoS often calculated as a ratio of ultimate stress induced in the mechanical component and the working stress. However, other factors such as the presence of stress concentrations, exposure to extreme environment (temperature, pressure, corrosion etc.), frequency of maintenance or the operational setting are important factors to consider while designing the equipment. As the current triaxial cell is designed to be used in beamlines, the following aspects were considered while assigning a FoS: a) the uncertainty in the strength of the rock b) the environment of the beamline, which are often confined spaces with a range of expensive and sensitive equipment and c) requirement of the triaxial cell to be portable and transparent to the beamline.

The FoS for the current design is based on the ratio of maximum stress induced in the cylindical component (the main body) of the triaxial cell to the ultimate compressive strength of the rock. The uncertainty in the denominator is to be taken into consideration when deciding on the FoS. This design was used for experimentation at two beamlines: a) IMAT at ISIS, a UK Science and Technology Facilities Council (STFC) facility in Harwell, Oxfordshire, UK and b) at National Institute of Standards and Technology (NIST) Center for Neutron Research (NCNR), a US government facility in Gaithersburg, MD, USA. Details of use and snapshots of results are discussed in Section 6.

3. Experimental test set up

Figure 2 shows the complete set-up including the ancillary equipment. The load is applied via a 100 kg-f (10 t) piston jack, which in this case was RLS 100, supplied by Powerteam §. This portable piston cylinder could also be a RCS 101 offered by Enerpac . The selection would be based on the required load to achieve the desired

§ Certain trade names and company products are mentioned in the text or identified in an illustration in order to adequately specify the experimental procedure and equipment used. In no case does such identification imply recommendation or endorsement by the National Institute of Standards and Technology, nor does it imply that the products are necessarily the best available for the purpose.

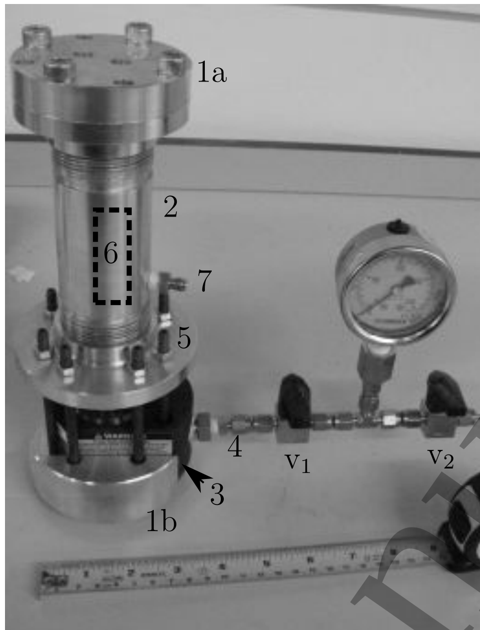

Figure 2. Experimental set-up. 1 a and b: platens 2. body of the cell to hold sample rock sample 3. loading ram (σ_1) 4. hydraulic oil supply for the ram 5. high tensile strength bolts 6. rock sample 7. confining pressure (σ_3) port.

deformation and the budget to build the test set up. The piston is connected to the manual hydraulic pump through a 316 Stainless steel seamless 3.175 mm (1/8 in) outer diameter and 0.7112 mm (0.028 in) thick tubing supplied by Swagelok (Part number: SS-T1-S-020-6ME) with maximum working pressure of 58.605 MPa (8500 psi). The key design aspect is the ability to isolate the pressure line after exerting required $\sigma_{\max}$ and $\sigma_{\min}$ on the rock sample. A two way valve is connected at close proximity to the piston (316 stainless steel quarter turn instrument plug valve with 3.175 mm (1/8 in) Swagelok tube fitting 0.1Cv - Part number SS-2P4T and working pressure of 20.6 MPa) and next to the valve is a pressure gauge (63 mm pressure gauge with lower fitting and dual scale 0 to 3000 psi and 0 to 200 Bar supplied by Omega Engineering UK, part number PGM-63L-3000PSI/200BAR) and another two way valve (same as previous). In order to change the $\sigma_{\max}$ on the rock, the two valves are opened and using the manual pump (Enerpac P141, single speed hydraulic pump). Once, required σ_{v} is reached, the valve nearer to the pump is closed, while the pressure in the gauge is monitored to ensure the σ_{v} on the rock is stable. The valve, v_1 is shut and the valve v_2 is opened to reduce the pressure in the line before disconnecting the compression fitting. Once isolated, the cell will retain the hydraulic pressure while a complete set of radiograms are acquired. This design of the system eliminates the necessity of flexible tubing that may be otherwise required to ensure smooth rotation of the cell while 2D radiograms are acquired for different angular rotation of the triaxial cell.

Figure 3 shows the cross section of the triaxial cell. It can be observed that the rock sample is supported by a sleeve, which ideally should be a fully florinated polymer.

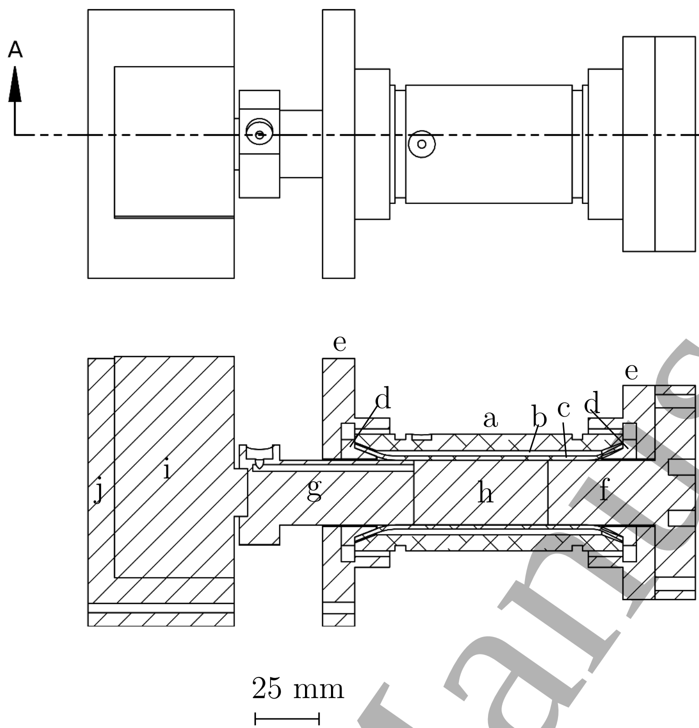

Figure 3. Triaxial cell. a. main body b. space for confining fluid c. Rubber sleeve d. collar e. end cap f. fixed platen g. moving platen (loading side) h. rock sample i. hydraulic jack j. housing for the hydraulic jack.

However, partially florinated polymer or for instance Viton could be used, especially if the fluids are likely to react with the sleeve. Another option that has been used in the past, although not as flexible as Viton , is a heat shrink tubing. The top platen is fixed and is secured by four to eight bolts. The lower platen is able to move and transfer load from the hydraulic jack to the rock sample. It also has fluid ports for injecting fluids into the rock sample. It is usual to have a distribution network of channel to the upstream platen to ensure the fluid is injected uniformly into the rock sample rather than two points but is omitted from the current design as it will reduce the area in contact with the rock sample and hence will not be able to apply load uniformly to the rock sample. The following sections will detail the design of each of the components shown in figure 3.

4. Design of various components of the triaxial cell

4.1. Main body

The main body is the pressure bearing component of the cell. It can be designed as a thick or thin cylinder based on the wall thickness, which in turn would depend on the intensity of the imaging beam. The maximum attenuation can be calculated by knowing the exact composition of the Aluminium alloy used, the chemical composition of the rock and the fluid in the pore spaces. Using mass attenuation data, the thickness of the main body spanning the length of the sample being imaged, for acceptable attenuation of the beam can be determined.

The material selected for the cell is Aluminium 6082-T6 alloy, as it has highest strength (nearly 240-250 MPa of proof strength and 300 MPa of tensile strength) amongst 6000 alloys. Furthermore, 6082 alloy has very good corrosion resistance and is commonly used in applications involving stress bearing components. One limitation of 6082 is the high manganese content and as Mn strongly activates with neutrons releasing a strong beta field making the sample handling immediately after imaging quite challenging. To overcome this issue, Aluminium 6061-T6 can be used. It is also to be noted that if strength is an absolute requirement- for instance- when testing extremely hard rocks, 7075 alloy may be an option but would radiate a strong beta radiation field due to Mn. One aspect that is noteworthy is the inclusion of other metals in the chosen alloy, for instance cobalt, would pose significant limitation in handling after the termination of the experiment due to the degree of activation.

The body of the triaxial cell is tubular with inside edges chamfered to house the collar that provides a seal with the rubber sleeve which in turn holds the rock sample in place (figure 3). The details of the other components will be discussed later. A fluid entry and exit port that houses a 3.175 mm (1/8 in) NPT fitting is placed closer to one end of the cell, to facilitate the hydraulic pressure for confining stress ($\sigma_{\mathrm{h}} = \sigma_{\mathrm{H}}$). The hole is positioned to ensure that it is sufficiently away from the rock sample (as shown in figure 4) for two reasons: a) it is designed to house a 3.175 mm (1/8 in) NPT stainless steel male to 3.175 mm (1/8 in) female compression fitting (of Swagelok type), which will have higher attenuation and if near the rock sample, it may affect the quality of the images acquired and b) if the images are truncated so as to contain only rock sample and tubular part of the cell, the 3D reconstructions from those 2D radiograms would be faster. The ends have a 46×2 mm threads to house the end caps.

The critical load bearing part of the experimental test set up is the main body as it is subjected to the confining pressure of the fluid as well as stress resulting from the dilation of the sample during testing. Therefore, finite element analysis of the load bearing main body was undertaken. Apart from testing the structural integrity, the finite element analysis is expected to inform the factor of safety in the design.

Figure 5(a) depicts the 3D model of main body created in SolidWorks software along with the imposed boundary conditions. The flat sides on the top and the bottom of the cell were assumed to be fixed as these are held in place with near zero allowable displacement during the test. In the real set up, the main body of the triaxial cell will also be subjected to axial tension due to the tightening of the bolts (shown by the number 5 in figure 2). The axial stress will in fact would increase the burst pressure. However, for the current Finite Element modelling exercise, the axial stress is ignored, which would result in lower burst pressure and therefore a higher factor of safety. The threaded hole where the 3.175 mm (1/8 in) NPT to Swagelok fitting for confining pressure is housed (No. 7 in figure 2) was fixed as the integrity of the fixture is ensured by selecting the correct fitting and appropriate depth of the thread. A uniform pressure was applied on

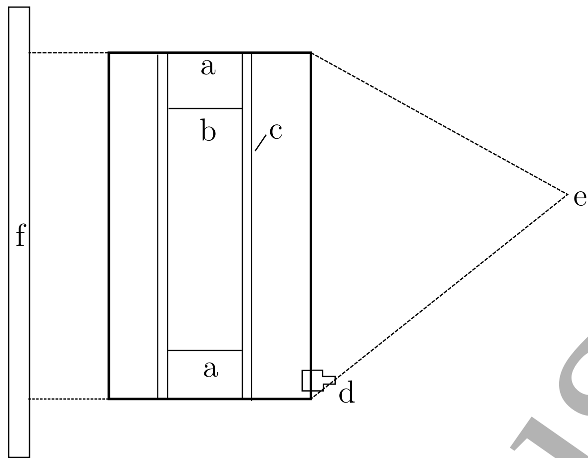

Figure 4. Triaxial cell with location of the NPT fitting for confining fluid. a. Platens b.Rock sample c. Rubber sleeve d. 3.175 mm (1/8 in) NPT fitting e. Source f. Detector.

the internal cylindrical surface, reflecting the application of confining pressure σ_3. It is to be noted that the internal pressure applied on the main body of the cell is one of the design parameter and can be used to optimise the cell design, especially in terms of its thickness. It is to be noted that, thickness of the cell/the enclosure is an important parameter for synchrotron and non-synchrotron based x-ray sources for imaging. However, the design is easily adaptable as the thickness of only main body needs to be altered to suit the energy in the imaging beamlines and phenomena of interest. In the current study, the cell was designed for an internal pressure of 10 MPa.

Figure 5(b) depicts the finite element mesh. To enable discretisation of all the features in the triaxial cell body, a free mesh was chosen and was optimised for convergence of displacement and stress.

Figure 5(c) shows the von Mises stress distribution within the main body of the triaxial cell and it can be noted that the maximum stress is near the hole that houses 3.175 mm (1/8 in) NPT fitting, indicating the effects of concentration of stress due to the removal of material and slightly reduced thickness. The maximum stress induced due to confining stress of 10 MPa was found to be 58 MPa. The factor of safety for the current design is 4.31, for a conservative yield strength of 6082 alloy as 250 MPa. It is to be noted that the thread recesses at both ends are chamfered and therefore are not contributing to any concentration of stress in those areas.

Figure 5(d) shows the resultant solid displacement within the main body of the triaxial cell, due to the applied internal pressure of 10 MPa. The shape of the distorted body is similar to other cylindrical vessels subjected to internal pressure.

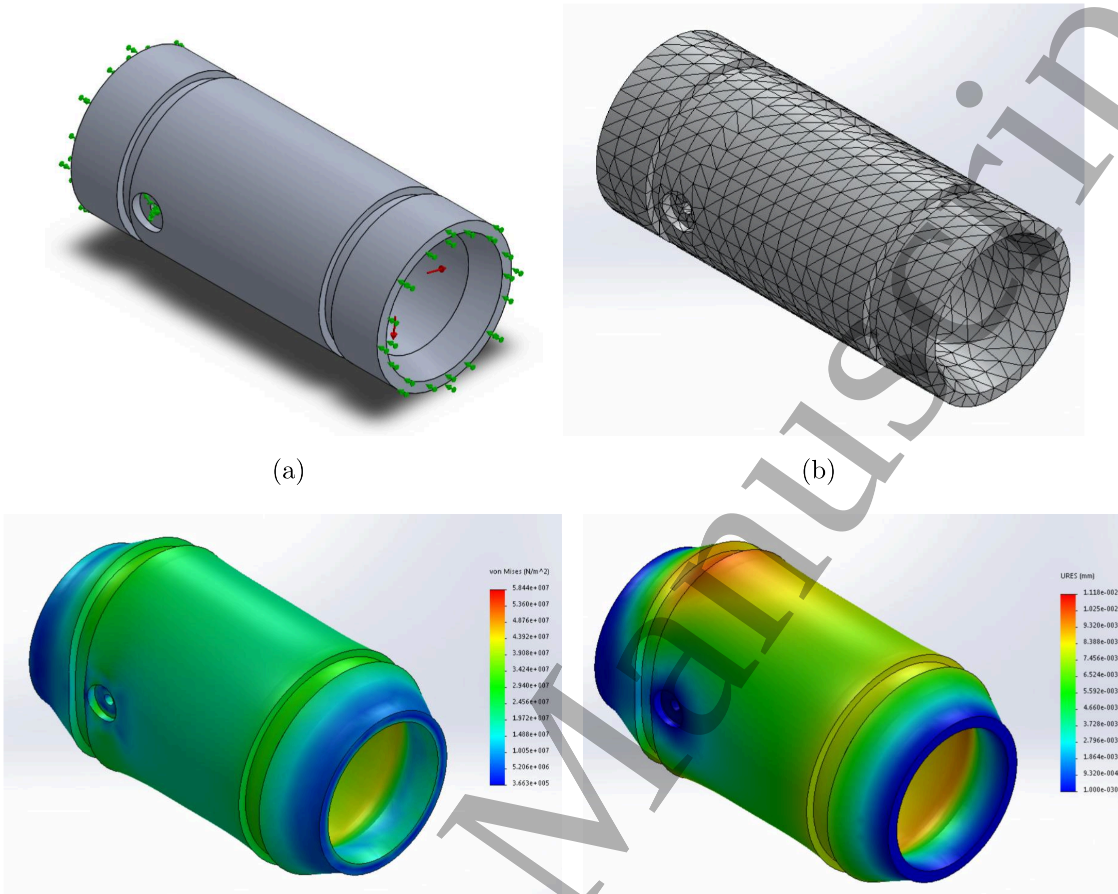

(a) (b)

(c) (d)

Figure 5. Triaxial cell with (a) boundary conditions, (b) Finite Element mesh, (c) von Mises stress and (d) deformation under internal pressure of 10 MPa.

4.2. Seal for the triaxial cell

The rock is held in place with a rubber sleeve (parts h and c respectively in figure 3). A SolidWorks model of the taper is shown in figure **??**. The taper on the conical section of the collar is identical to that on the cell main body, which allows positioning of the sleeve in way that it is compressed between the main body and the collar providing a surface seal. It is to be noted that the edges of the conical part must not be sharp to avoid any possible damage to the rubber sleeve. A fillet was applied to the edges to make it smooth. The taper angle angle must be selected so as to avoid sharp corners and retaining the ability to slide the rubber sleeve on the collar for the assembly which provides the seal for the confining pressure. The sliding action of the conical element also enables the process of gradually settling up of rubber to provide seal as described in the Section 5 below.

The end cap (figure 6) is designed to hold the collar and the sleeve in place. The end caps are threaded and are designed to match the thread on the body. In the current

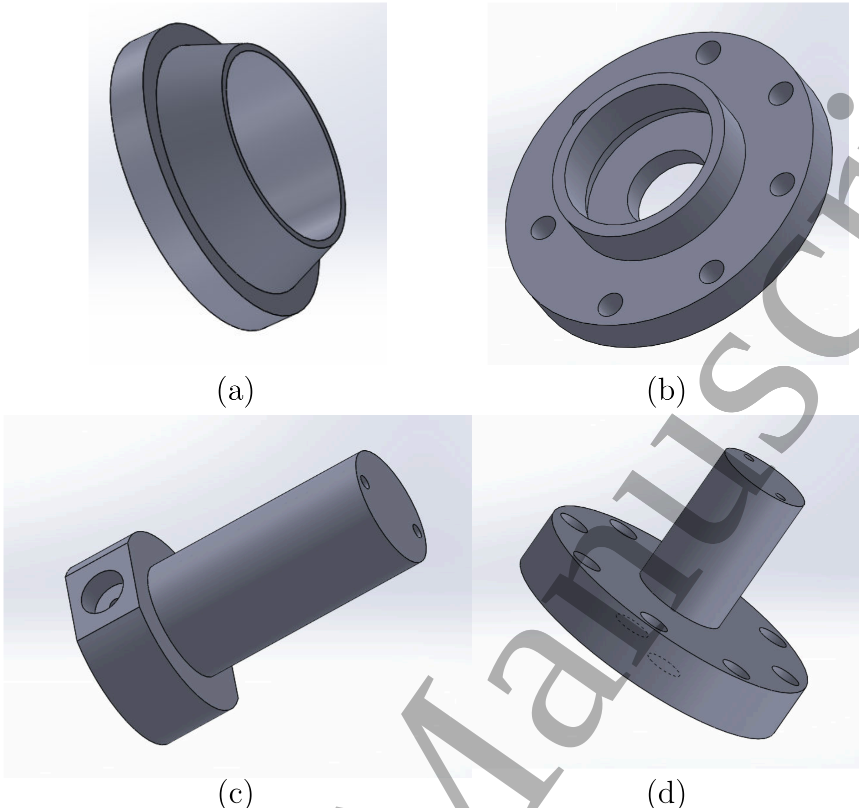

Figure 6. Parts of Triaxial cell (a) collars that provide seal, (b) endcaps; platens for (c) loading and (d) fixed side.

design 46×2 mm threads are machined on both end caps and the main body of the cell. As shown in figure 3, the end caps threads on the main body and during the turning movement, pushes the collar firmly into the main body, thereby forming a seal for the confining fluid (space is indicated by b in figure 3). The ends caps also has eight equispaced holes at angle 45° threaded to M6 to secure the platen (discussed in the Section 4.3 below).

4.3. Platens

Platens (plate like structures with protrusions) have two functions in this cell:

a to impart load or to apply displacement boundary conditions,

b to facilitate the flow of fluids through the rock sample sample (design was incorporated in the current set up but was not used in the demonstration).

There are two platens for the triaxial cell. Firstly, there is a floating platen at the loading side of the cell (figure 3 and 6). It consists of a single cylindrical member with an extension at the end, primarily designed to limit the possible displacement, in case needed; and to enable the flow of fluids into and out of the rock. The extended portion has two ports each of depth 12 mm to house 3.175 mm (1/8 in) NPT male connector to compression fitting (of Swagelok type). The length of the platen would depend on

the rock sample and estimated compression of the sample before failure. Two holes of diameter 3 mm run parallel to the longitudinal axis of the platen which can be used to inject fluids into the rock sample. The spacing between the holes can also be varied to suit specific experimental requirements. For the current design the spacing between the ports was maximised and hence was set to 19 mm.
Figure 6 shows the fixed side platen. The cylindrical part of the platen is identical to the loading side platen but the cylindrical part ends in a flange which is use to secure the platen to the end cap (figure 3). The flange has eight clear hole at 45º as well to match the end cap. Depending on the load only four bolts may be sufficient to secure the platens.

4.4. Plumbing

The plumbing of cell with ancillary equipment was carried out with 3.175 mm (1/8 in) stainless steel tubing supplied by Swagelok®. The fittings were of 316 Stainless Steel are rated in accordance with ASME Code for Pressure Piping B31.3. The pressure ratings for the fittings used are: maximum pressure of 68.9 MPa (male) and 44.7 MPa (female).

4.5. Loading mechanism

The load is applied using an RLS 100 hydraulic loading jack, supplied by Powerteam®. The maximum load that can be applied using RLS 100 is 89000 N (10 t). It is relatively light weight, making the test set up very portable. It is housed in an Aluminium housing (figure 2). The RLS 100 has two holes which can be matched with the bottom platen using through bolts through the housing, spacing between the loading side end cap and the piston of RLS100 can be maintained. Before securing the bolts on the loading side end cap, it is advisable to ensure that there is enough space for the piston to travel so that the rock can be compressed to failure. A two way valve is placed inline and can be used to isolate the cell, once desired axial load is applied on the rock sample. This isolation enables easy rotation of the cell along the longitudinal axis and hence makes it convenient set up for use in fixed source (x-ray or neutron) 3D tomography. Similar arrangement can also be used for confining stress ($\sigma_\mathrm{h} = \sigma_\mathrm{H}$).

4.6. Bill of materials

Table 2 details the itemised cost (in British Pound Sterling) of the components used in the triaxial cell set up. It is to be noted that the prices include value added tax (UK and EU, where applicable) and educational discount (variable as it is in accordance with commercial negotiation between the University and individual suppliers) offered by suppliers to the University of Aberdeen. The total cost does not include the cost of manufacturing of the equipment at the University of Aberdeen's workshop and subsequent modifications undertaken at the workshops at NIST and IMAT. Furthermore, the materials were procured at different points in time and therefore the cost in table 2 should be taken with caution.

Table 2. Bill of materials for the triaxial cell set up. The unit and total cost stated are in British Pound Sterling.

Component	Quantity	Unit cost	Total cost
Power Team RLS100 Cylinder	1	204.41	204.41
1/16 in OD × 0.020 in WT 316/316: Tubing (SS-T1-S-020-ME)	6	10.69	64.13
SS Quarter-Turn Instrument Plug Valve, 3.175 mm (1/8 in) Swagelok Tube Fitting, 0.10 Cv (SS-2PT4T)	2	69.19	138.38
63 mm pressure gauge with lower fitting and dual scale 0 to 3000 psi and 0 to 200 Bar (PGM-63L-3000PSI/200BAR)	1	70.88	70.88
Enerpac Hand pump	1	276.73	276.73
Viton Sleeve (1 m)	1	408.75	408.75
Minature Quick-Connect Body, 0.05 Cv in Swagelok tube fitting (SS-QM2-B-200SS)	1	56.65	56.65
Swagelok Tube fitting Union Tee 3.175 mm (1/8 in) Tube OD (SS-200-3-SS)	2	25.94	51.88
SS Swagelok Tube Fitting, Reducer, 1/16 in × 3.175 mm (1/8 in) Tube OD (SS-100-R-2)	1	14.18	14.18
SS Swagelok Tube Fitting, Male Connector, 3.175 mm (1/8 in) Tube OD × 3.175 mm (1/8 in) Male NPT(SS-200-1-2)	1	7.98	7.98
Stainless Steel Pipe Fitting, Reducing Bushing, 3/8 in Male NPT × 3.175 mm (1/8 in) Female NPT, Swagelok Fittings (SS-6-RB-2)	1	6.75	6.75
Aluminium stock	1	75.00	75.00
Total			1375.69

4.7. Errors and uncertainty

The accuracy of the vertical load and confining stress will depend on the accuracy with which the pressure gauge can be read. In case of PGM-63L-3000PSI/200BAR pressure gauge, which was used in the current set up, the accuracy of the instrument is 1.6% of span (200 bar). Parallax error is another source of error in the application of load on the sample. The least count of this pressure gauge is 10 bar and hence the uncertainty in the measurement of applied pressure would be 10 bar. For experiments that require a high degree of precision in the application of loads, it is recommended that digital pressure transducers are used to monitor the pressure. Use of a pressure controller could also be a viable option especially if pressure sensitive rocks are to be tested.

5. Discussion on the design and operation

The design of this triaxial cell is simple and the components are easy to manufacture in a standard machine shop and can be assembled with relative ease. The key aspect of the cell is the formation of the seal for the confining fluid between the collar and the body of the cell. The following is the sequence adapted for pressure testing of the cell, and is based on the stress relaxation of Viton elastomer sleeve:

(i) A dummy (diameter 25.4 mm and 70 mm in length) was introduced into the main body and the end cap was gently tightened to be finger tight. Nitrogen was then injected into the confining pressure space to maintain a pressure of 0.7 MPa ($\approx$ 100 psi).

(ii) The cell was isolated by closing the valve next to the confining pressure port. If the pressure had reduced over a short period of time ($\approx$ 0.03 MPa over 5 minutes), then it was very likely due to a leak somewhere which was identified and the end caps were tightened until the leak stopped. Leaking nitrogen from the triaxial cell can be detected by pouring a few drops of soapy water at the threaded portions of the main body of the cell (which was found to be the most common pathway for the leak) and at locations where different parts have been joined.

(iii) The triaxial cell was then left for approximately 24 hours with the pressure monitored with time. If the drop in pressure is in excess of 0.07 MPa (10%) then the leak was identified through the use of soapy water and in the absence of observable leak the end caps were to be tightened as the drop in pressure was attributed to very slow release of gas through the end cap assembly.

(iv) Once the pressure is sustained over 24 hours, fresh gas from from source was injected into the confining pressure chamber to increase the pressure to 1.5 MPa and the aforementioned process is repeated.

The intention of this exercise is to obtain a permanent shape of Viton sleeve by incremental application of pressure. The steps suggested above for the setting of sleeve, are purely based on the experience of working with similar type of triaxial cells in the laboratory for over 15 years.
A threaded hole at the bottom of the piston holder may be included to facilitate the mounting of the cell on the rotation table/stage (as seen in figure 7(b)).
It is to be noted that with appropriate instrumentation such a suitable portable

Linear Variable Differential Transformer (LVDT), to measure axial displacement and connection to a more sophisticated servo-controlled hydraulic system, the test set up can be used for triaxial test in the laboratory. However, detailed discussion on such adaptation is beyond the scope of this paper, which focuses on the use of this test set up in beamline experiments.

6. On functionality of the proposed triaxial cell in beamlines

The triaxial test set up has been used for imaging fractures within various rocks at two beamlines (a) at IMAT, STFC-ISIS facility, UK [25, 26] and (b) at the NIST Center for Neutron Research (NCNR), the triaxial cell (with suitable wall thickness) was used in the NeXT beamline [27]. The following sections details the discussion on the performance of the triaxial cell in these beamlines.

6.1. IMAT beamline, ISIS facility, UK

Figure 7 depicts the positioning of the cell on the IMAT beamline, ISIS facility, UK. The cell was 15 cm in front of the detector. The position of the cell with respect to

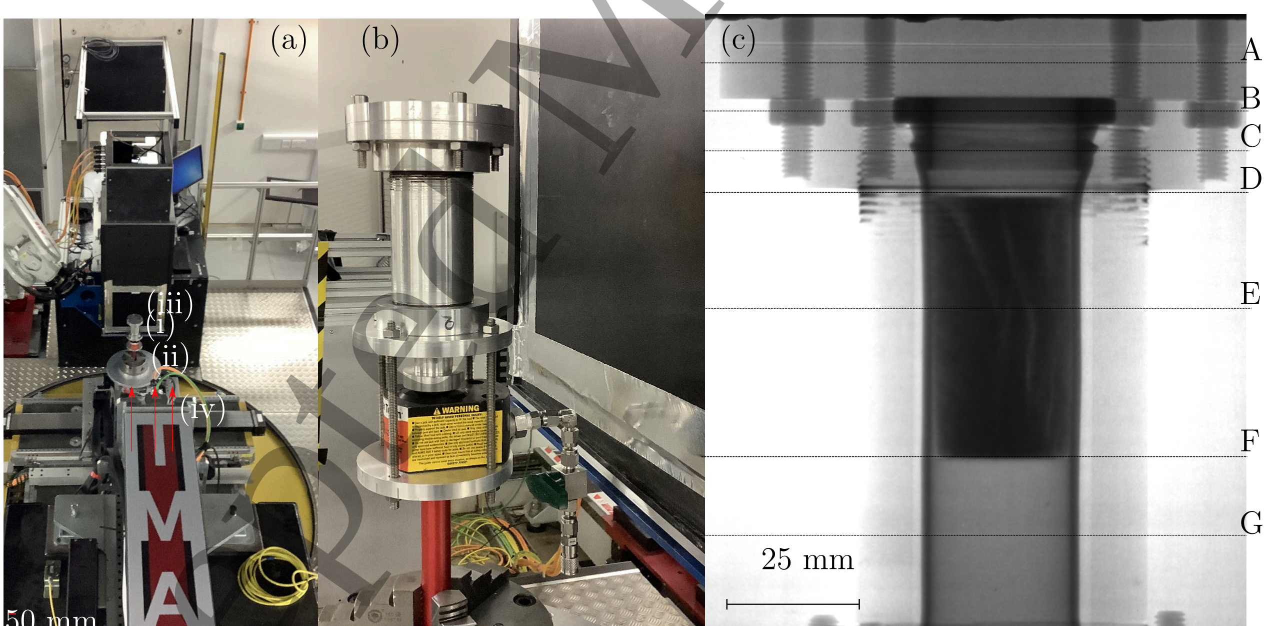

Figure 7. (a) Triaxial cell mounted on IMAT, ISIS facility. (i). Cell (ii). Stage (iii). Detector and (iv). Direction of the beam. (b) Close up of the cell with ancillary fittings to contain the axial load on the sample and (c) Neutron radiogram of the cell containing a Lochaline rock sample of diameter 25 mm.

the detector was adjusted using a Laser, mounted near the entrance of the beam in the experiment hall. An elbow connector, shown in 7(b), was used to minimise the distance the triaxial cell can be positioned in front of the detector and to enable the triaxial cell to be isolated, once the axial stress was applied. The configuration of the elbow connector comprising of a two way valve and Swagelok Minature Quick-Connect connector which enables the isolation of cell, while maintaining the axial stress. Figure 7(c), depicts one of the radiogram obtained for the water saturated rock sample - a rock extremely rich in Si from side of Loch Aline in North Western Argyll in Scotland [28]. Initial trial to image dry rock were unsuccessful due to very low attenuation of neutrons when passed through Si-rich rock. It can be noted from the figure 7(c) that a clear outline of the fractures appears to have propagated due to the application of the load. The voxel resolution obtained on IMAT was $\approx 120\mu m$.

Figure 8 depicts the variation of attenuation, I/I_o, along the sections of the triaxial cell highlighted in figure 7 (c) with A through to G. The reference $r = 0$ mm refers to the centre of the triaxial cell. Following observations were made:

- Along A in figure 7, at $r = -40$ mm, the $I/I_o = 0.38$ was measured from beamline experiments which was due to the high tensile strength bolt of diameter 6 mm. With the density of material taken as 7.9 g cm^{-3}, the mass attenuation coefficient, μ/ρ was found to be 0.2 cm^2 g^{-1}, which is in agreement with those reported in the literature for Fe [22].
- For section indicated by line A and $r = 0$ mm, the attenuation of the beam is due to Aluminium alone travelling through the 80 mm diameter of the top platen. Using the density of Al as 2.7 g cm^{-3}, μ/ρ was found to be 0.047 cm^2 g^{-1}, which is comparable to those reported for Al in [22].
- The I/I_o measured along section B, C and D can be used to confirm the presence of Aluminium or iron (due to the bolts).
- At $r = 0$ mm in section E, the $I/I_o = 0.09$ is a combination of beam attenuation due to Al in cell body, Si in grain and H in porespace of the rock sample and in Viton sleeve.
- At $r = 0$ mm in section G, the $I/I_o = 0.448$, which is predominantly due to Al and H in Viton sleeve.
- Although F is taken at the interface of rock and the Al of the loading side platen, the $I/I_0 = 0.236$ at $r = 0$ mm, is less than those observed at G but greater than the H dominated attenuation at E. It does suggest that the attenuation at $r = 0$ mm in section F is due to a combination of Al in triaxial cell, H in rock and Viton sleeve and Si in rocks.
- The gradual change in the attenuation at a few locations along all the sections can be noted, which is attributed to the combination of material and its thickness along the direction of the passing beam.

In conclusion, it was noted that the design of the triaxial cell is suitable for its intended purpose of using it in a beamline for identification of specific characteristics of geomaterials subjected to triaxial state of stress and the attenuation of beam at various spatial location is largely as expected from the materials used in its manufacture.

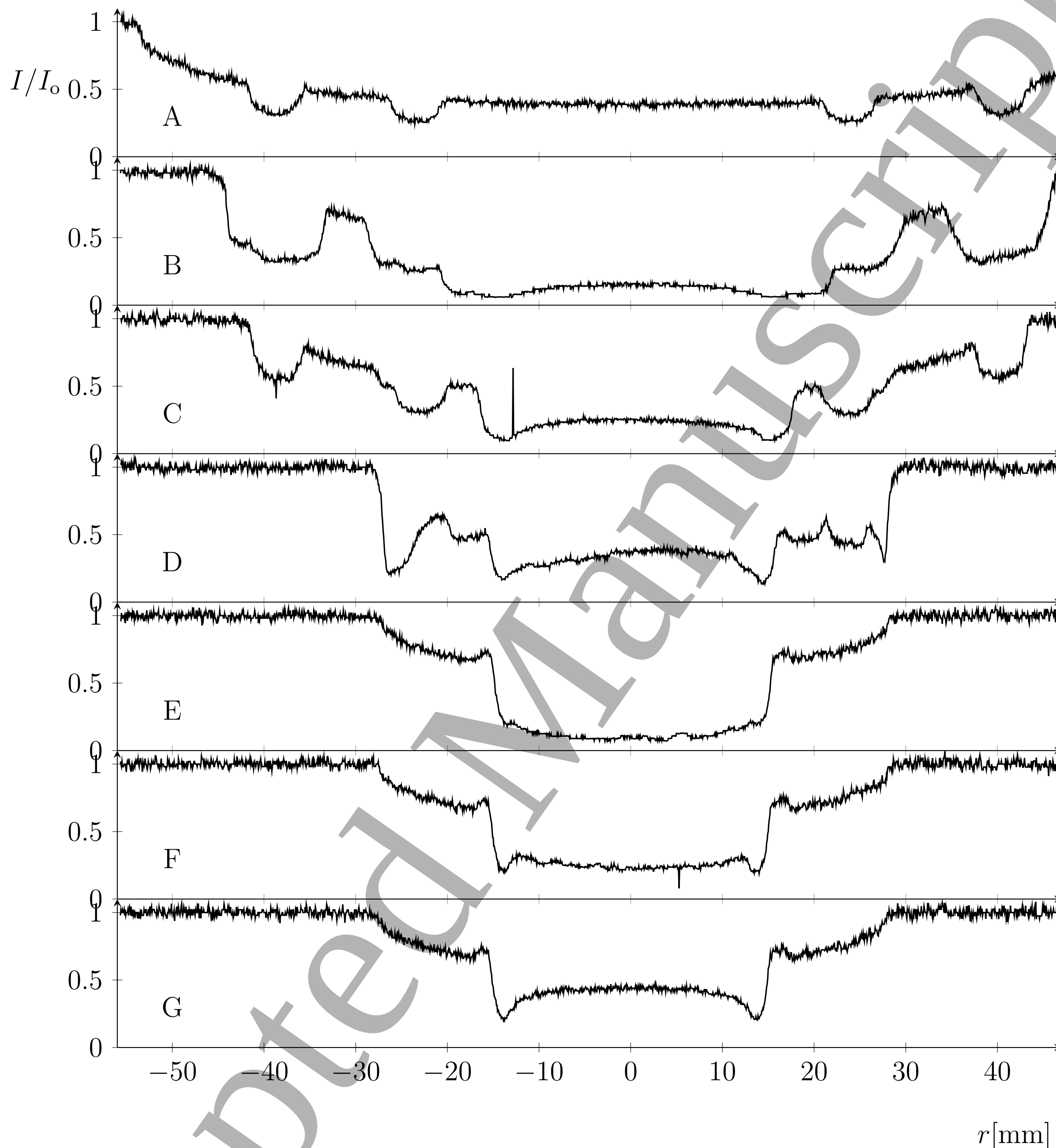

Figure 8. Variation of I/I_o along selected sections of triaxial cell.

6.2. BT2, NIST Center for Neutron Research, NIST, MD, USA

Experiments were conducted at BT2 beamline at NIST Center for Neutron Research at Gaithersburg, MD, USA. The BT2 facility is equipped with x-ray imaging facility in addition to neutron imaging facility, thereby enabling the collection of x-ray and neutron images simultaneously [27]. At BT2, due to the constraint of x-ray attenuation, the wall thickness needed to be reduced. The triaxial cell was therefore modified to remove the material on the cylindrical part of the cell body in order to have a wall thickness of 2 mm. Figure 9(a) depicts the modified cell with reduced wall thickness. Structural analysis of 3-D model was conducted to ensure that the design was safe under operating load.

Figure 9 (b) and (c) depicts the x-ray and neutron radiograms of Locharbriggs rock

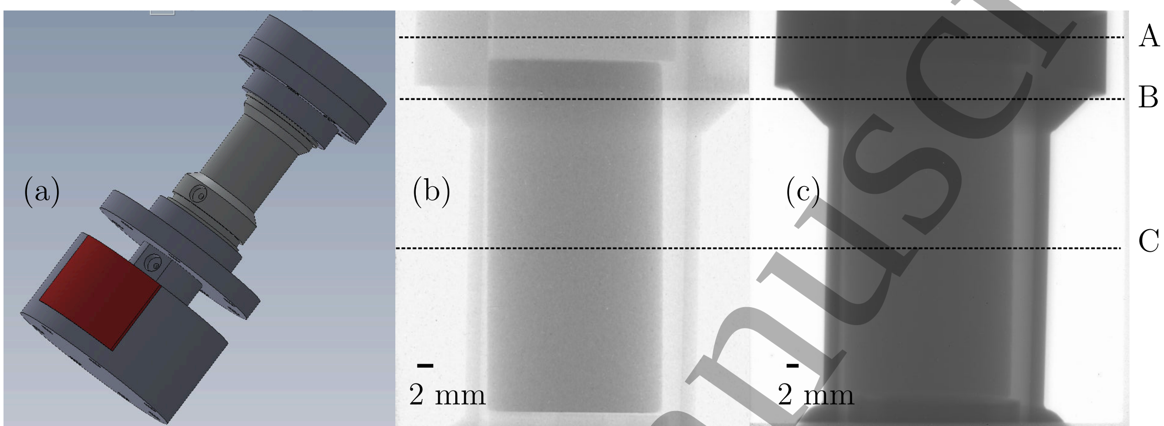

Figure 9. Cell in beamline at BT2, NCNR facility. a. 3D image of modified design of triaxial cell. (b) Neutron and (c) X-ray radiograms of Locharbriggs sandstone.

sample - a high porosity quartz rich (88%) red standstone of Permian origin, sourced from a quarry near Dumfries in south-west of Scotland [29]. The high neutron flux at BT2 and relatively lower Si content of Locharbriggs sandstone enabled imaging experiments to be carried out without saturating it with water.

The obtained voxel resolution for neutron was $\approx$ 30 μm and for that of x-ray was $\approx 30\mu$m. It is to be noted that Viton sleeve was not used for these experiments. Figure 6.2 depicts the attenuated beam through the triaxial cell. The following observations were drawn:

- Section A in figure 9 (b) and (c) is composed mainly of Al. At $r = 0$ mm, the centre of triaxial cell, $I/I_o = 0.65$ and therefore $\mu/\rho = 0.032$ cm^2 g^{-1}, which is lower than those reported in [22]. However, for x-ray the attenuation ratio at the same location, $I/I_o = 0.035$ and $\mu/\rho = 0.248$ cm^2 g^{-1}, greater than those interpolated from the data from [23].
- For $r = 0$ mm at Section C, which primarily consist of dry rock, i.e. Si, $I/I_o = 0.556$ for neutron beam and $I/I_o = 0.1$ for x-ray. The attenuation is mainly due to the Si in the rocks with contribution of Al and taking the density of Si to be 2.33 g cm^{-3}, the $\mu/\rho = 0.049$ cm^2 g^{-1} for neutrons and $\mu/\rho = 0.040$ cm^2 g^{-1} for x-ray, which is slightly lower than those reported by [23], with the variation attributed to the presence of Al and other metallic inclusions in the main body of the triaxial cell.

6.3. Limitations of the current design of triaxial cell and suggestions for improvement

The following are some of the identified limitations of the current design.

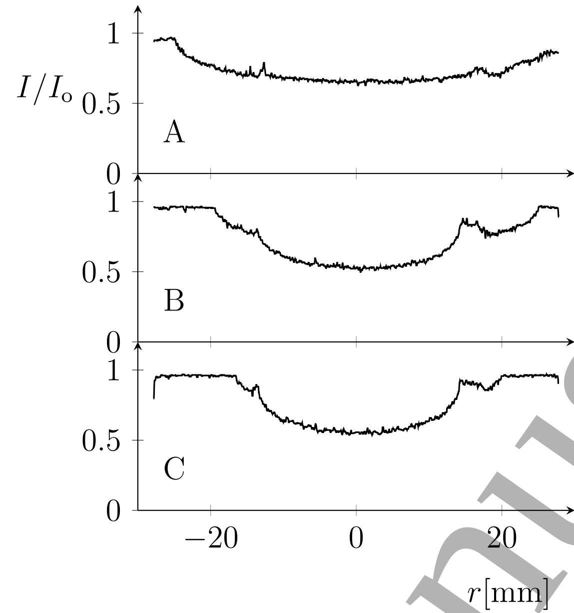

Figure 10. Attenuation on neutron beam through the triaxial cell at BT2, NCNR.

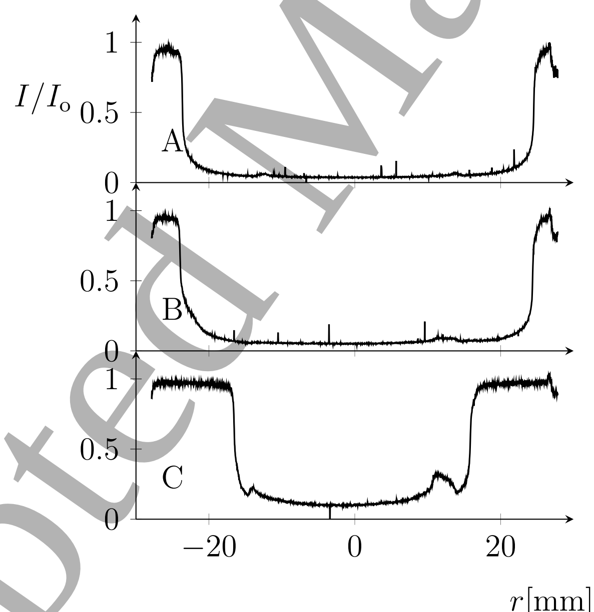

Figure 11. Attenuation on x-ray beam through the triaxial cell at BT2, NCNR.

- The mechanical response of rock is sensitive to the rate of strain used in the triaxial test. The International Society of Rock Mechanics recommends a strain rate of 20 millistrain per hour. However, the current test set up only enables the application of instantaneous load. A suggestion would be to replace the manual hydraulic pump with a pressure controller that can enable application of axial displacement, while maintaining a constant rate of strain. This would enable reproduction of identical laboratory triaxial conditions in the beamlines.

- The continued dilation of rock due to the increase in applied axial load would increase the radial displacement which would in turn increase the pressure in the confining fluid chamber. Therefore, a further improvement would be to connect the confining pressure to a device that could control the confining stress during the experiment, for instance, a pressure controller. However, the plumbing needs to be carefully considered as it would be the major limiting factor for most beamlines that have rotating stages. One suggestion would be investigation of the use of multi-channel hydraulic or pneumatic rotary unions that would allow the rotation of the stage while maintaining pressure connectivity between the confining pressure chamber and the controller.

7. Conclusions

A portable triaxial rock sample holder design is presented, which can be used to image flow and deformation under triaxial state of stress. The design is versatile and can be modified to suit different beamlines that have stationary source while the triaxial cell is rotated from 0 to 180 or 360 degrees. The current design ensures that the cell is isolated under stress for imaging, thereby eliminating long flow lines which may not be conducive in some experimental scenarios. The triaxial cell was used for imaging the deformation characteristics and fracture propagation in clastic rocks at two beamlines. The μ/ρ computed for Al, Si and Fe was found to be in close agreement with those reported in the literature.

8. Acknowledgements

The development of the cell was supported by the Research and Teaching Excellence Fund of the School of Engineering, University of Aberdeen. Experiments at BT2, NCNR were supported by UK Engineering and Physical Sciences Research Council grant number EP/N021665/1, NIST and the Physical Measurement Laboratory. Experiments at IMAT were supported by the UK STFC, Experiment number: 1910331 (https://doi.org/10.5286/ISIS.E.RB1910331).

References

[1] N. Kardjilov, A. Hilger, I. Manke, M. Strobl, M. Dawson, and J. Banhart. New trends in neutron imaging. *Nucl. Instrum. Methods Phys. Res., Sect. A*, 605:13–15, 2009.

[2] J. Kumar, A. Attridge, P.K.C. Wood, and M.A. Williams. Analysis of the effect of cone-beam geometry and test object configuration on the measurement accuracy of a computed tomography scanner used for dimensional measurement. *Meas. Sci. Technol.*, 22:035105, 2011.

[3] J.S. Lee, B.M. Weon, and J.H. Je. X-ray phase-constrast imaging of dynamics of complex fluids. *J. Phys. D: Appl. Phys.*, 46:494006, 2013.

[4] D. Bauer, H. Chaves, and C. Arcoumanis. Measurements of void fraction distribution in cavitating pipe flow using x-ray CT. *Meas. Sci. Technol.*, 23:055302, 2012.

[5] W.J. Richards, M.R. Gibbons, and K.C. Shields. Neutron tomography developments and applications. *Appl. Radiat. Isot.*, 61:551–559, 2004.

[6] M. Dierick, J. Vlassenbroeck, B. Masschaele, V. Cnudde, L. Van Hoorebeke, and A. Hillenback. High-speed neutron tomorgaphy of dynamic processes. *Nucl. Instrum. Methods Phys. Res., Sect. A*, 542:296–301, 2005.

[7] P. Vontobel, E. Lehman, and W.D. Carlson. Comparison of X-ray and neutron tomography investigations of geological materials. *IEEE Trans. Nucl. Sci.*, 52(1):338–341, 2005.

[8] M. Wilding, C.E. Lesher, and K. Shields. Applications of neutron computed tomography in the geosciences. *Nucl. Instrum. Methods Phys. Res., Sect. A*, 542:290–295, 2005.

[9] B. Winkler, A. Kahle, and B. Hennion. Neutron radiography of rocks and melts. *Physica B*, 385-386:933–934, 2006.

[10] S. Iglauer, A. Paluszny, C. Pentland, and M. Blunt. Residual CO_2 imaged with X-ray micro-tomography. *Geophys. Res. Lett.*, 38:L21403, 2011.

[11] E. Perfect, C.-L. Cheng, M. Kang, H.Z. Bilheux, J.M. LaManna, M.J. Gragg, and D.M. Wright. Neutron imaging of hydrogen-rich fluids in geomaterials and engineered porous media: A review. *Earth Sci. Rev.*, 129:120–135, 2014.

[12] C. Degueldre, H. Pleinert, P. Maguire, E. Lehman, J. Missimer, J. Hammer, K. Leenders, H. Boeck, and D. Townsend. Porosity and pathway determination in crystalline rock by positron emission tomography and neutron radiography. *Earth Planet. Sci. Lett.*, 140:213–225, 1996.

[13] K. H. Hellmuth, M. Siitari-Kauppi, P. Klobes, K. Meyer, and J. Goebbels. Imaging and analyzing rock porosity by autoradiography and Hg-porosimetry/X-ray computertomography-Applications. *Phys. Chem. Earth (A)*, 24(7):569–573, 1999.

[14] J. Behnsen, O.O. Blake, R.J. Cernik, and P.J. Withers. Identifying microcracks in multi-phase crystalline rocks by X-ray CT. In *iCT conference*, 2014.

[15] P. Christe, M. Bernasconi, P. Vontobel, P. Turberg, and A. Parriaux. Three-dimensional petrographical investigations on borehole rock samples: a comparison between X-ray computed- and neutron tomography. *Acta Geotech.*, 2:269–279, 2007.

[16] E. Hoek and J.A. Franklin. Simple triaxial cell for field or laboratory testing of rock. *Transactions of Institution of Minerals and Metallurgy*, 77:A22–26, 1968.

[17] K.K. Fu, M.C. Yang, and K.L. Wood. Design principles: Literature, review, analysis and future directions. *ASME J. Mech. Des.*, 138:101103–1–13, 2016.

[18] I. Mohedas, S. R. Daly, and K.H. Sienko. Requirements development: Approaches and behaviors of novice designers. *ASME J. Mech. Des.*, 137:071407–1–10, 2015.

[19] J. Fender, L. Graff, H. Harbrecht, and M. Zimmermann. Identifying key parameters for design improvement in high-dimensional systems with uncertainity. *ASME J. Mech. Des.*, 136:041007–1–10, 2014.

[20] P. Kraemer and A. Weckenmann. Multi-energy image stack fusion in computed tomography. *Meas. Sci. Technol.*, 21:045105, 2010.

[21] J. Banhart, A Borbély, K Dzieciol, F Garcia-Moreno, I Manke, N Kardjilov, A Kaysser-Pyzalla, M Strobl, and W Treimer. X-ray and neutron imaging - complementary techniques for materials science and engineering. *IJMR*, 101(9):1069–1079, September 2010.

[22] H. Berger. Neutron radiography. *Annu. Rev. Nucl. Sci.*, 21:335–364, 1971.

[23] J.H. Hubbell and S.M. Seltzer. NIST Standard Reference Database 126: X-ray mass attenuation coefficients. Online, July 2004. Accessed 20 December 2020.

[24] D. Fusseis, H. Steeb, X. Xiao, W. Zhu, I.B. Butler, S. Elphick, and U. Maeder. A low-cost X-ray-transparent experimental cell for synchrotron-based X-ray microtromography studies under geological reservoir conditions. *J. Synchrotron Rad.*, 21:251–253, 2014.

[25] G. Burca, W. Kockelmann, J. A. James, and M.E. Fitzpatrick. Modeling of an imaging beamline at the ISIS pulsed neutron source. *J. Instrum.*, (10), 2013.

[26] W. Kockelmann, G. Burca, J. Kelleher, S. Kabra, S.-Y. Zhang, N.J. Rhodes, E.M. Schooneveld, J. Sykora, D.E. Pooley, J.B. Nightingale, F. Aliotta, R.C. Ponterio, G. Salvato, D. Tresoldi,

C. Vasi, J.B. McPhate, and A.S. Tremsin. Status of the neutron imaging and diffraction instrument imat. *Phy. Procedia*, 69:71–78, 2015.

[27] J.M. LaManna, D.S. Hussey, E. Baltic, and D.L. Jacobson. Neutron and X-ray Tomography (NeXT) system for simulataneous, dual modality tomography. *Rev. Sci. Instrum.*, 88(11):113702, 2017.

[28] D.W. Humphries. The upper Cretaceous white sandstone of Loch Aline, Argyll, Scotland. *P. Yorks. Geol. Soc.*, 33(4):47–76, 1961.

[29] I.O. Ojala, B.T. Ngwenya, I.G. Main, and S.C. Elphick. Correlation of microseismic and chenical properties of brittle deformation in Locharbriggs sandstone. *J. Geophys. Res. Solid Earth*, 108(B5):2268, 2003.